



# Oxidation of pyrite ( $\text{FeS}_2$ ) and troilite ( $\text{FeS}$ ) impurities in kaolinitic clays after calcination

Franco Zunino · Karen Scrivener

Received: 23 March 2021 / Accepted: 16 December 2021 / Published online: 24 December 2021  
© The Author(s) 2021

**Abstract** Valorisation of locally available clays for producing blended cements is crucial for a widespread adoption of sustainable binders incorporating these materials. In some places, clays can be intermixed with small amounts of iron sulfides, which could eventually expand in the alkaline media of concrete and lead to cracking if clay particles are sufficiently fine. This study explored the stability of iron sulfides, namely troilite and pyrite, during calcination of clays and their influence in reactivity. It was found that both troilite and pyrite decompose and oxidize into hematite under typical calcination conditions for clays. Furthermore, there is no negative influence of the presence of iron sulfide phases on the reactivity of calcined clays. This shows that these clays are suitable for use in blended cements, provided that adequate quality control is conducted to ensure a complete decomposition of the iron sulfide phases.

**Keywords** Sulfides · Calcination · Expansion · Reactivity · Sustainability

## 1 Introduction

The substitution of clinker by supplementary cementitious materials (SCMs) is the most effective way to reduce the carbon footprint associated with the Portland cement industry [1]. Among them, calcined clays and limestone are particularly interesting due to their widespread availability [1, 2]. The combination of limestone and calcined clays in cement ( $\text{LC}^3$ : limestone calcined clays cement) enables the clinker factor to be reduced down to 50% while reaching comparable strength to OPC at 7 days [3].

Clay minerals are made up of a stack of alternating layers [4]. Kaolinitic clays are the most promising alternative for calcined clay production, as they exhibit higher reactivity than others such as illite and smectites [5, 6]. Kaolinite dehydroxylates between 400–650 °C, generating an amorphous aluminosilicate phase called metakaolin. Clays with kaolinite content of 40% or above are suitable for use in  $\text{LC}^3$  cements [6, 7].

Kaolinite is normally intermixed in natural clay deposits with other associated minerals such as quartz, feldspars and iron oxides [8]. Iron oxides are responsible for the reddish coloration seen in some natural clays [9]. In some cases, minerals that decompose upon calcination such as carbonates or aluminum hydroxides (gibbsite) can be found [10, 11]. Iron sulfides (pyrite, pyrrhotite and/or troilite) can also be

---

F. Zunino (✉) · K. Scrivener  
Laboratory of Construction Materials, EPFL STI IMX  
LMC, École Polytechnique Fédérale de Lausanne,  
1015 Lausanne, Switzerland  
e-mail: franco.zunino@epfl.ch



found in some kaolinitic clay deposits, intermixed in relatively minor amounts (< 5% by mass).

Iron sulfides can also be found in some aggregates used in concrete manufacture. It has been seen that their presence leads to expansion and cracking due to the formation of iron hydroxides. The cracking patterns are similar to the ones observed due to alkali silica reaction [12]. The expansion has been observed even with low concentration of iron sulfides in the aggregates (0.28% by volume). Both quantity and distribution of sulfides play a role in the observed expansion. This raises a concern regarding the suitability of kaolinitic clays intermixed with iron sulfides to be used as SCMs.

On heating, iron sulfides transform into other mineral phases. This process is in general complex and involves several simultaneous transformations [13]. Furthermore, the type of phases formed and extent of the transformations are strongly dependent on atmosphere (oxidizing/reducing) and particle size of the calcined material [14–16]. Given the high volatility of iron sulfides at high temperature, they are expected to oxidize to form iron oxide (hematite,  $\text{Fe}_2\text{O}_3$ ) [14].

This study assessed the decomposition of iron sulfides, namely pyrite ( $\text{FeS}_2$ ) and troilite ( $\text{FeS}$ ), when intermixed and calcined with kaolinite under temperature and residence time conditions commonly used to produce reactive calcined clay. The mineralogy of the resulting calcined material was characterized, and its suitability for use in cement-based materials is discussed.

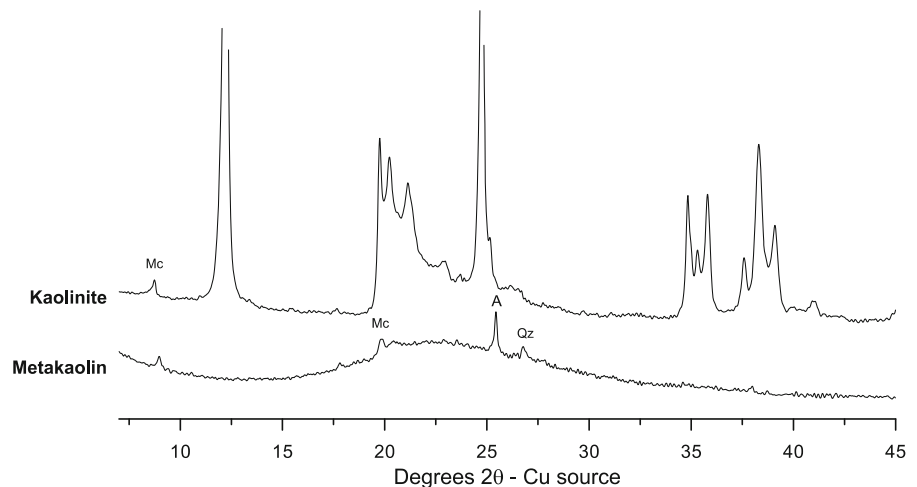
## 2 Materials and methods

### 2.1 Raw materials

A relatively pure Kaolinite was used as base material to produce systems with controlled amounts of intermixed iron sulfide impurities. This had a kaolinite content of 91.4% determined by thermogravimetric analysis (TGA) [7]. The other minerals contained in the base material were muscovite, anatase and quartz, as seen in the X-ray diffraction (XRD) pattern shown in Fig. 1. After calcination at 800 °C for 30 min, full dehydroxylation of kaolinite was observed. After calcination, the associated minerals remained unaltered, as observed in Fig. 1.

Iron (II) sulfide ( $\text{FeS}$ , CAS 1317-37-9, SigmaAldrich) and iron (II) disulfide ( $\text{FeS}_2$ , CAS 12068-85-8, Fischer) were used as raw minerals to intermix with kaolinite to produce clays with different contents and mineral forms of iron sulfides. Both reagents were ground in a disc mill for 1 min to reduce the particle size distribution (PSD) of the powders. The resulting PSDs were measured by laser diffraction using water as a dispersant (refractive index 1.73, imaginary component 0.1), and are shown in Fig. 2 along with the distribution measured for kaolinite (optical model taken from [17]). It can be seen that despite using the same grinding process, some large particles (above 100  $\mu\text{m}$ ) remained present in the  $\text{FeS}_2$  material. As it will be seen later, this did not interfere with the overall thermal decomposition of the material. XRD analysis showed that  $\text{FeS}$  corresponds to

**Fig. 1** XRD patterns of kaolinite and metakaolin obtained after calcination at 800 °C for 30 min. The main two reflections of kaolinite have been cut to enhance the visibility of the smaller reflections



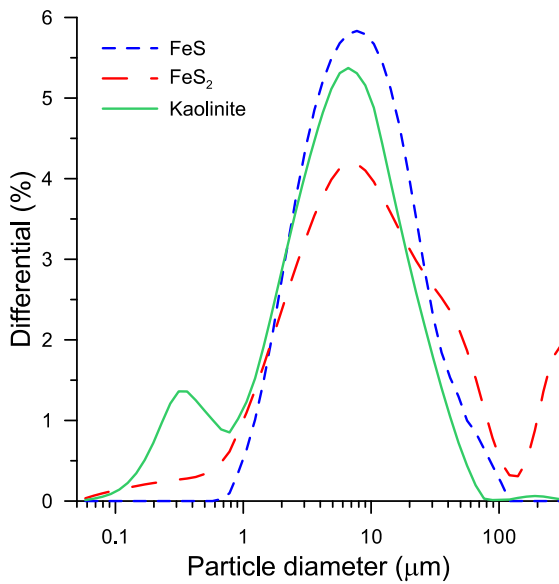


**Fig. 2** Particle size distribution of kaolinite and ground FeS/FeS<sub>2</sub> and kaolinite used in this study

troilite (the stoichiometric mineral variant from the pyrrhotite group, Fe<sub>1-x</sub>S, with  $x$  between 0 and 2), while the FeS<sub>2</sub> used corresponds to pyrite.

Model systems were prepared to study the transformation of iron sulfides on calcination when intermixed with kaolinite, and their influence on the reactivity of the calcined material. Kaolinite and FeS/FeS<sub>2</sub> were intermixed at 5–10–20% mass replacement of kaolinite by each of the iron sulfide minerals. While 20% is significantly higher than the contents of iron sulfide normally found in natural clays, it was used as an extreme case to ensure that full decomposition of sulfides takes place even at high concentrations. To achieve a uniform blending of the powders, the different proportions of kaolinite/iron sulfides were placed inside plastic containers in a Turbula blender (simultaneous roll and shake) for 24 h.

In addition to the synthetic kaolinite + FeS/FeS<sub>2</sub> described above, three natural kaolinitic clays containing pyrite impurities were studied to validate the results obtained from the model systems. The natural clay samples were dried at 105 °C for 72 h and subsequently ground in a disc mill for 30 s. The kaolinite content, measured by TGA, was 18.9, 19.7 and 20.8% for code named clay P1, P2 and P3, respectively. The PSDs of the three natural clays are shown in Fig. 3.

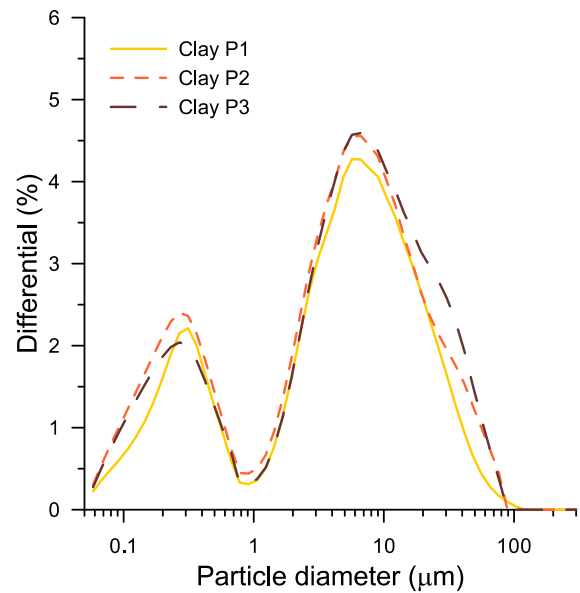


**Fig. 3** Particle size distribution of natural kaolinitic clays containing pyrite (FeS<sub>2</sub>) impurities

## 2.2 Experimental methods

Model clay systems (kaolinite + FeS/FeS<sub>2</sub>) and natural clays were calcined in a laboratory (static) furnace. In addition, a sample of pure troilite and pyrite was also calcined to study the mineralogical changes in these phases after calcination. 50 g of powder were placed in alumina crucibles, which were placed in the furnace. The furnace was heated to 800 °C, which took around 40 min (heating ramp of approximately 20 °C/min), the samples were held at 800 °C for 30 min. These conditions were established to ensure full dehydroxylation of kaolinite and achieve the maximum potential reactivity in the obtained calcined clays [2, 7].

TGA was used to measure the kaolinite content of the calcined materials and also to characterize the decomposition of iron sulfide species upon heating. In the case of kaolinite content assessment, 40 mg of powder was placed in alumina crucibles and heated up to 1000 °C at 10 °C/min rate, under a protective N<sub>2</sub> (reducing) atmosphere flowing at 30 mL/min. In the case of iron sulfides, it is known that atmosphere has an influence on the transformations that these minerals experience upon heating [13]. For this reason, the protective atmosphere used was air (oxidizing) flowing at 30 mL/min, in order to reproduce the

environment during the calcination in the static furnace and in a real industrial calcination process.

XRD was conducted on powder samples to characterize their mineralogical composition. Measurements were made on back loaded powder samples to reduce the effects of preferred orientation. The samples were measured in Bragg–Brentano mode using a X’Pert PANalytical diffractometer with CuK $\alpha$  source operated at 45 kV and 40 mA with a  $1/2^\circ$  soller slit. Samples were scanned from  $7^\circ$  to  $70^\circ$   $2\theta$  with a step size of 0.0167  $2\theta$  using a X’Celerator detector, resulting in an equivalent time per step of 60 s. Commercial software (HighScore Plus version 4.6) coupled with the ICCD database were used for phase matching and Rietveld refinement.

The reactivity of each of the calcined samples was measured by isothermal calorimetry, following the ASTM C1897 procedure (R3 test) [18] which enables to measure the reactivity of the material and its potential to contribute to strength in cementitious systems. In this procedure, calcined clay is mixed with portlandite, calcium carbonate, potassium sulphate, potassium hydroxide and water, and put into glass ampoules inside the calorimeter at  $40^\circ\text{C}$ . The signal was recorded for 120 h.

Morphological changes in iron sulfide minerals before and after calcination were characterized by high-resolution scanning electron microscopy (SEM). Powder samples were mounted on a carbon tape and coated with 4.0 nm of iridium using a tilted-

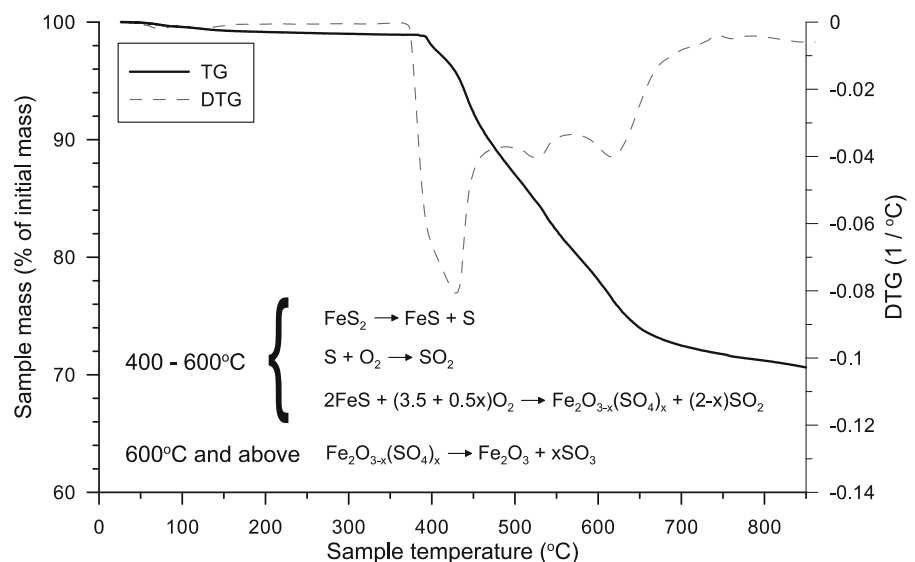
rotatable stage. Iridium produces crystallites of about 3–4 nm in size, ensuring that morphological features are observable at high magnification. A Zeiss GeminiSEM 300 was used operating at 2.0 kV and a working distance of 3.0 mm. An in-lens secondary electron (SE) detector was used as it offers the best resolution in this microscope.

### 3 Results and discussion

#### 3.1 Thermal decomposition of pyrite ( $\text{FeS}_2$ ) and troilite ( $\text{FeS}$ ) under oxidizing conditions

The thermogravimetric curve showing the transformation of pyrite ( $\text{FeS}_2$ ) between 30 and  $850^\circ\text{C}$  (range of interest for clay calcination) under an air atmosphere is shown in Fig. 4. Between  $400$  and  $600^\circ\text{C}$ , three overlapped decompositions (seen as three peaks in the derivative DTG curve) take place.  $\text{FeS}_2$  is decomposed into troilite and/or pyrrhotite ( $\text{FeS}$  and/or  $\text{Fe}_{1-x}\text{S}$ ) and sulfur gas, which simultaneously combines with oxygen forming  $\text{SO}_2$  gas. The  $\text{FeS}$  formed can also take up oxygen from the surrounding air and form iron sulfate minerals in this temperature range [13]. The occurrence of this transformation depends on the partial pressure of oxygen surrounding the material [19]. Above  $600^\circ\text{C}$ , decomposition of iron sulfate takes place, leading to the formation of iron oxide (hematite,  $\text{Fe}_2\text{O}_3$ ). The occurrence of these

**Fig. 4** TG and DTG curves of pyrite under oxidizing (air) atmosphere conditions



transformations depends on the atmosphere and the particle size of the material [15]. Nevertheless, if a temperature in the range of 700 °C is reached (lower temperature boundary required to ensure dehydroxylation of kaolinite [2]) the end product will be hematite under sufficiently oxidizing (air) conditions, irrespective of the specific transformation path followed [14, 15].

Troilite (FeS) or pyrrhotite ( $\text{Fe}_{1-x}\text{S}$ ) follows a different transformation path compared to pyrite, Fig. 5. Between 30 and 450 °C a mass increase is observed, associated with the uptake of oxygen from the atmosphere to form iron sulfate phases [13, 16]. Above 450 °C, remaining FeS combines with oxygen to form hematite, releasing  $\text{SO}_2$  gas. Above 600 °C, iron sulfate is decomposed to form hematite, similarly as in the case of pyrite [20].

The different intermediate transformations on heating for pyrite and troilite lead to significant differences in the loss on ignition (LOI) values for each mineral at reaching 850 °C. In the case of pyrite, the final weight of the sample is about 70% of the initial mass, while in the case of troilite the final weight of the sample is 97% of the initial mass. In this case, there is a lower mass loss associated with sulfur release, which is simultaneously offset partially by the uptake of oxygen.

The mineralogical composition of the initial and end (calcined) products of pyrite and troilite, formed after calcination at 800 °C for 30 min in a lab furnace,

was studied by XRD. The diffraction patterns are shown in Fig. 6. Despite the strong absorption of copper radiation by iron which leads to a decrease in the signal-to-noise ratio, reflections can still be identified for a qualitative analysis.

The troilite (FeS) used contained minor amounts of metallic iron, which also becomes oxidized after calcination. Only hematite is observed in the calcined FeS pattern. In the case of the pyrite ( $\text{FeS}_2$ ) used, minor amounts of quartz and clinochlorite were identified in addition to pyrite in the raw material. Clinochlorite is decomposed after calcination, while quartz is still observable in the calcined sample along with hematite. In the case of  $\text{FeS}_2$ , minor amounts (3–5% by mass) of troilite (FeS, intermediate product upon decomposition of pyrite, see Fig. 4) were still detected in the calcined sample, indicating that the oxidation process was not complete. This was only observed when pure pyrite was calcined. In real cases, the amount of pyrite present will be considerably lower if the material is properly homogenized prior to calcination. At lower concentrations, full oxidation of pyrite into hematite is achieved under the same calcination conditions, as it will be shown in subsequent sections.

As previously shown, the numerous processes take place during the heating of pyrite/troilite in an oxidizing atmosphere. An alternative approach could involve chemical oxidation of sulfides using hydrogen

**Fig. 5** TG and DTG curves of troilite under oxidizing (air) atmosphere conditions

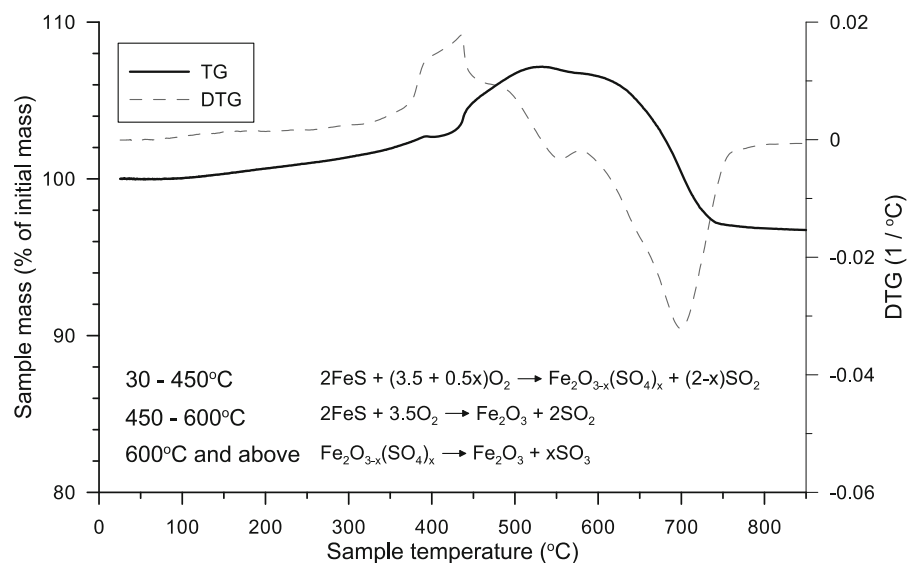
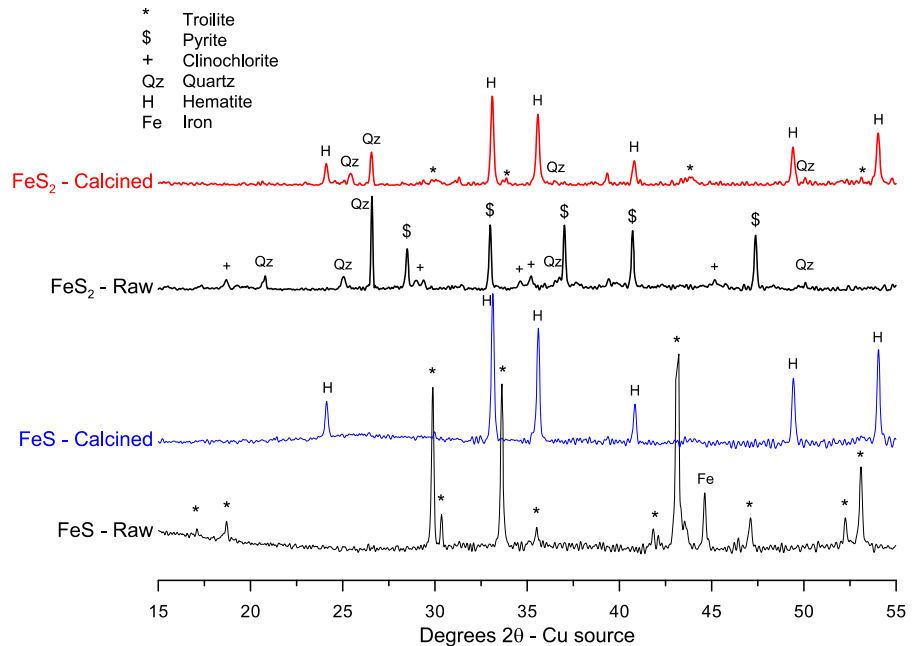


**Fig. 6** Diffraction patterns of FeS and FeS<sub>2</sub> minerals before (raw) and after (calcined) calcination at 800 °C for 30 min in a laboratory furnace



peroxide, however, the suitability of this method to treat clays is unclear and should be further explored.

There is general agreement in previous studies that the decomposition of iron sulfides and the consequent liberation of sulfur gases leads to the formation of porous particles, where gas diffusion takes place [13, 14]. This effect is also used as part of the expansion process in the production of expanded clay as lightweight aggregates. Furthermore, this porosity influences oxygen diffusion and the ultimate oxidation of the material into hematite. Dunn et al. described three mechanisms for the oxidation of pyrite upon heating [15]:

1. Oxygen diffusion into the sulfide particle (low temperature mechanism). Oxidation occurs via shrinking core mechanism. The oxide delays further diffusion of oxygen and transformation into hematite.
2. Above  $\sim 500$  °C, if pyrite is not fully oxidized, the mechanism changes to one controlled by the pyrolytic decomposition of pyrite to pyrrhotite. The released sulfur produces considerable porosity, which assists further oxidation into hematite.
3. If heating conditions are vigorous enough, particles can ignite upon heating. Temperature exceeds pyrolytic decomposition temperature, and

promotes fast oxidation. This mechanism is encouraged by small particles.

The morphology of raw and calcined iron sulfides was studied by SEM. Micrographs of raw and calcined samples are shown in Fig. 7. Both troilite and pyrite have smooth particle surfaces before calcination. After calcination, more porosity is observed, and the deposition of a liquid-like residue in the surface of the particles suggests that some degree of melting took place. The porosity and formation of this deposit leads to an increase in specific surface area of the resulting hematite. In the case of pyrite, an increase of surface area of 45% (1.07 to 1.45 m<sup>2</sup>/g) was observed, while in the case of troilite the surface area of the calcined material was almost double (1.38 to 2.59 m<sup>2</sup>/g) the initial value.

### 3.2 Kaolinite-pyrite and kaolinite-troilite model systems

#### 3.2.1 Mineralogical composition after calcination

The mineralogical composition of the model systems (kaolinite + 5–10–20% FeS/FeS<sub>2</sub>) after calcination in the lab furnace (800 °C for 30 min) was assessed by XRD. The diffractograms are shown in Fig. 8. It can be observed that in all cases, full dehydroxylation of

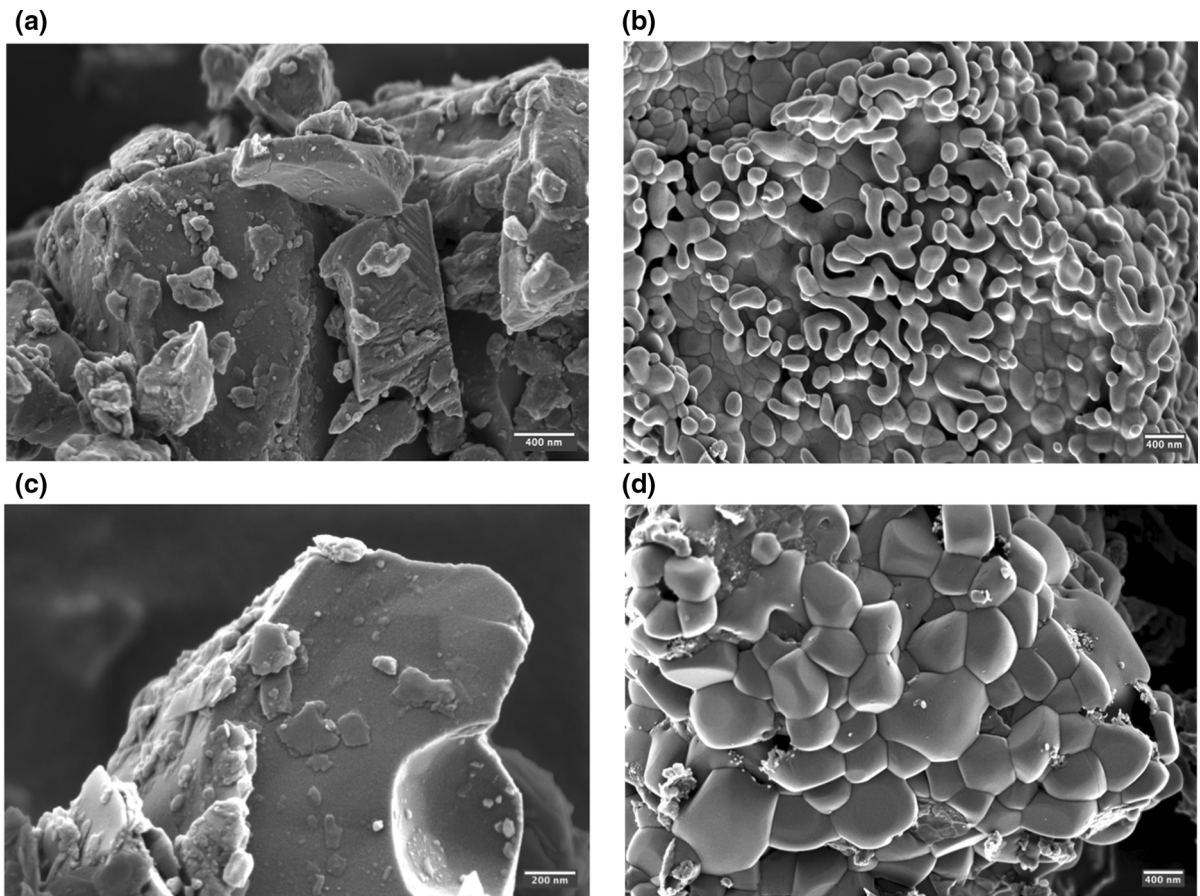
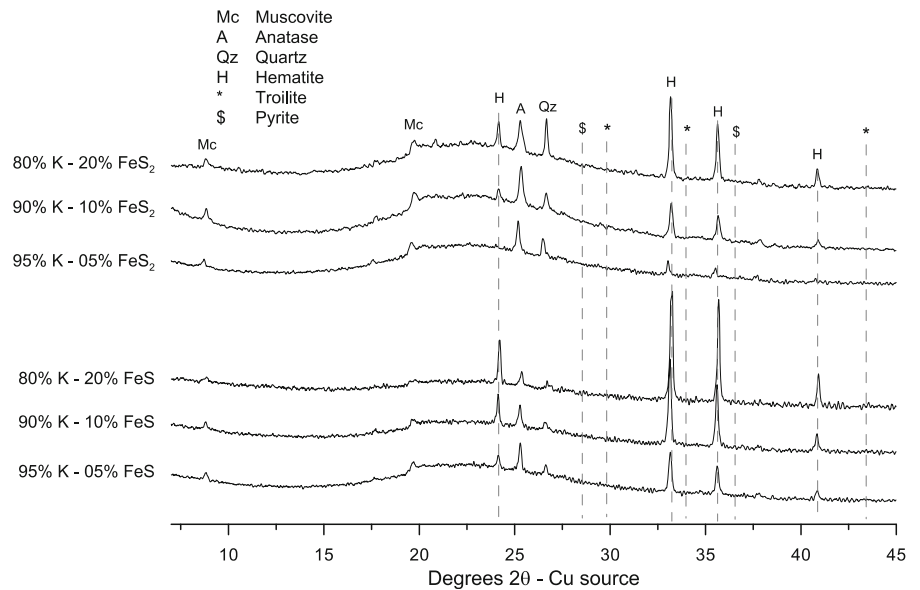


**Fig. 7** Micrographs (SE) of raw (a) and calcined (b) troilite (FeS) and raw (c) and calcined (d) pyrite (FeS<sub>2</sub>) samples

**Fig. 8** Diffraction patterns of model clay systems (kaolinite + 5–10–20% FeS/FeS<sub>2</sub>) after calcination at 800 °C for 30 min in a laboratory furnace. The lines of troilite and pyrite that are not overlapped with other phases are shown to confirm decomposition



kaolinite was achieved, as the peaks of kaolinite are no longer seen. The impurities found in the original kaolinite used in this study (muscovite, anatase and quartz) are observed in all calcined samples. Both pyrite and troilite oxidized completely into hematite, and no traces of residual iron sulfides were observed in any of the calcined clays. Higher amounts of hematite are seen in the FeS systems compared to the corresponding FeS<sub>2</sub> ones. This is associated with the smaller mass loss of troilite compared to pyrite, higher iron content in FeS (64% by mass) as compared to pyrite (47% by mass). Thus, for an equal mass replacement of kaolinite by FeS<sub>2</sub>/FeS, more iron-bearing phases remain after calcination in the FeS systems.

### 3.2.2 Reactivity

The reactivity of the model calcined clays was assessed using the ASTM C1897 method. The cumulative heat curves up to 120 h are shown in Fig. 9. The Metakaolin content is the main factor controlling the heat released during this test by calcined clays [7]. The curve obtained for pure metakaolin (MK) is presented as reference, along with scaled curves representing an idealized MK dilution at 10% (0.9MK) and 20% (0.8MK) replacement levels. All the calcined materials that initially contained iron sulfide minerals exhibit

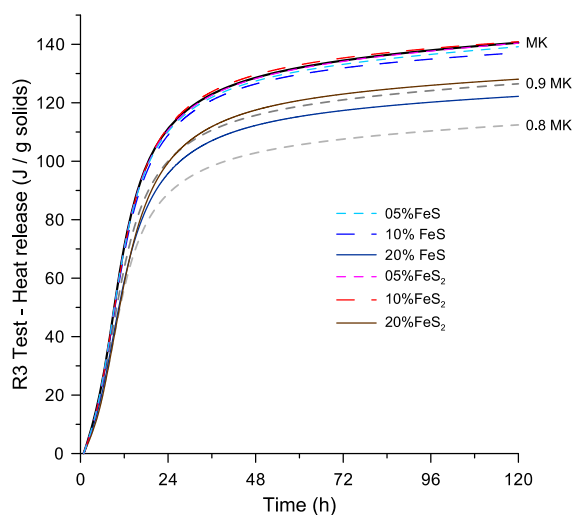


**Fig. 9** Reactivity assessment of calcined clays using isothermal calorimetry (ASTM C1897 method)

slightly higher reactivity than what would be expected given their metakaolin content. The differences between FeS and FeS<sub>2</sub> at the same replacement level (measured in the raw material) are associated with the different weight loss experienced by both minerals upon calcination, leading to different degrees of dilution of the calcined material.

Overall, the calcination conditions used (800 °C for 30 min) led to a full oxidation of iron sulfides into hematite, while enabling a highly reactive metakaolin to be obtained. Hematite is a stable mineral at room temperature, and as other iron oxides it has an extremely low solubility in aqueous media [21]. The solubility of hematite further decreases in alkaline solutions and thus, it can be safely incorporated in cement-based materials.

Calcination trials were conducted at lower temperatures (650 °C and 700 °C for 30 min) for the synthetic clay system with 10% pyrite addition. Despite the lower temperatures, pyrite was not observed in the diffraction patterns of the calcined material. In the case of 650 °C, dehydroxylation of kaolinite was not complete. Consequently, achieving full dehydroxylation of kaolinite could be considered as an equivalent control measure to ensure that sulfides are completely oxidized during calcined clay production. Even in cases where a small amount of iron sulfides may remain in the calcined material, the high degree of dispersion of these phases reduces the likeliness of expansion phenomena in concrete, as previously shown by Schmidt et al. [12].

### 3.3 Mineralogy and reactivity of natural clays containing pyrite

The observations on model kaolinite + iron sulfide systems show that under common calcination conditions aimed to maximize metakaolin reactivity, both pyrite and troilite completely oxidize to form hematite, eliminating the potential durability issue associated with their incorporation in concrete. To further validate these results, three samples of natural kaolinitic clays containing pyrite were analyzed in the same way as with the model systems. Figure 10 shows the diffraction patterns of each of the clays before (raw) and after calcination at 800 °C for 30 min.

In addition to kaolinite, the natural raw clays contain as associated minerals: muscovite, some minor amounts of gypsum (1.1, 1.5 and 1.1%



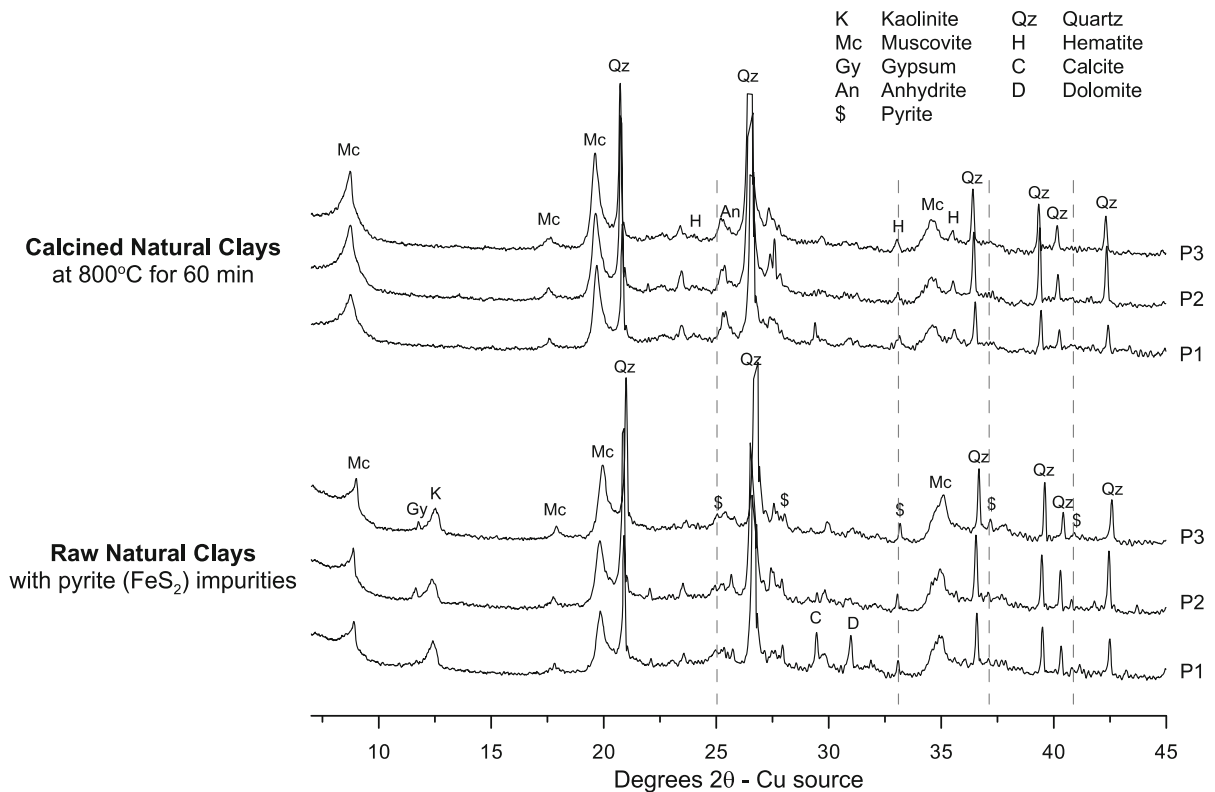


**Fig. 10** Diffraction patterns of natural clays containing pyrite (\$\$). Both raw clays (bottom) and calcined clays (top) are shown

determined by refinement for samples P1, P2 and P3 respectively) and quartz. Clay P1 also contains calcite (4.0%) and dolomite (1.7%). Calcium carbonate impurities can lead to the formation of an amorphous calcium aluminosilicate that precipitates on top of the kaolinite particles [10]. The pyrite content of samples P1, P2 and P3 was determined as 0.5, 0.5 and 0.7% respectively as measured by XRD. These values are significantly lower compared to the model systems studied. Nevertheless, the aim of verifying the findings on natural clays is to see if artificial intermixing of pyrite makes a difference on the observed oxidation process compared with naturally occurring clays.

After calcination, the peaks associated with kaolinite are no longer visible, indicating full dehydroxylation of the clay. Gypsum dehydrates and consequently, anhydrite peaks are seen instead. Muscovite remains invariant after calcination, as in the model systems (Fig. 6). The peaks of pyrite are no longer visible in any of the calcined clays. Instead, hematite reflections appear in all of the materials, in agreement with the results obtained in the model systems. Consequently,

the oxidation of pyrite in natural clays leads to the formation of the same products under equal calcination conditions as compared to lab-intermixed pyrite-kaolinite systems.

Figure 11 shows the thermal decomposition of clay P1 measured by TGA (air atmosphere). This clay was selected as it contains carbonate minerals; thus, more decomposition processes take place during calcination. The decomposition of kaolinite and the decarbonation of calcite/dolomite are clearly visible. By comparison with Fig. 4, it can be noticed that the decomposition of pyrite overlaps with the dehydroxylation of kaolinite, and consequently it cannot be identified accurately. Thus, TGA alone (without coupled analysis of released volatiles) is not a suitable technique to assess/quantify the presence of pyrite in natural clays and to verify the oxidation of this mineral after calcination. Instead, the qualitative XRD analysis shown in Fig. 10, is a more suitable approach to characterize these materials.

Figure 12 shows the reactivity assessment of the three natural calcined clays using the ASTM C1897

**Fig. 11** TG/DTG curve of natural clay P1, indicating the dehydroxylation of kaolinite and the decarbonation of calcium carbonates

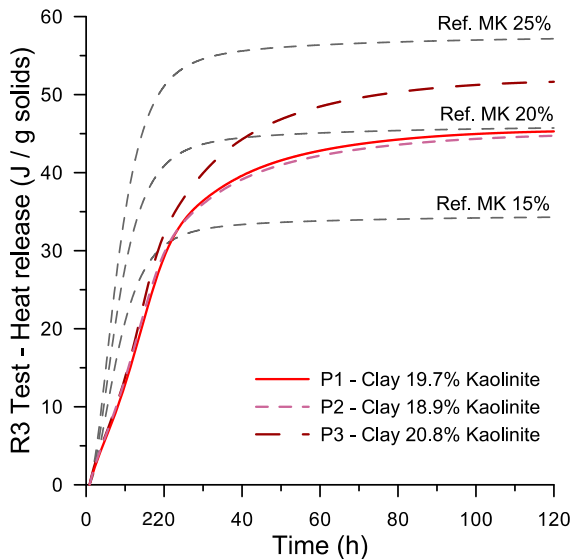
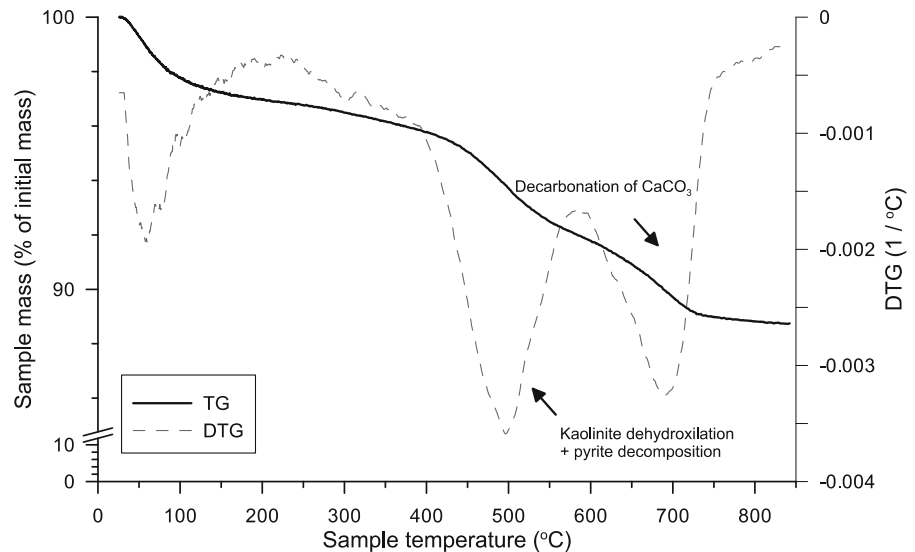


**Fig. 12** Reactivity assessment of natural calcined clays P1, P2 and P3 using isothermal calorimetry (ASTM C1897 method)

procedure. Dashed lines corresponding to idealized dilution curves of calcined clays with 25, 20 and 15% metakaolin are included for reference. As seen, all the natural calcined clays exhibit a reactivity in the expected range for their kaolinite contents. Like the model clay systems, there is no negative influence of the presence of pyrite on the final reactivity of the material, as long as proper dehydroxylation of kaolinite is achieved.

#### 4 Conclusions

This paper studied the suitability of using kaolinitic clays containing iron sulfides (pyrite and troilite) as sources of SCMs. As these minerals are known to cause expansion related cracking in concrete, the stability of these phases after calcination of the clay was the main focus of this study. Based on the results presented, the following conclusions can be drawn:

1. Pyrite ( $\text{FeS}_2$ ) and troilite ( $\text{FeS}$ ) oxidised in an air atmosphere when subjected to common calcination conditions for calcined clay production ( $800^\circ\text{C}$ , 30 min), leading to the formation of hematite ( $\text{Fe}_2\text{O}_3$ ) and the release of  $\text{SO}_x$  gas during the process. Calcination temperatures as low as  $650^\circ\text{C}$  was shown to be effective to fully oxidise pyrite in synthetic clay systems.
2. The presence of iron sulfides in raw clays does not have a negative influence on the reactivity of the calcined clays obtained.
3. X-ray diffraction is a suitable technique to assess the presence of iron sulfides in raw clays and to subsequently confirm that the oxidation of these minerals is completed after calcination. Equivalently, complete dehydroxylation of kaolinite can be taken as an indication of complete oxidation of sulfides intermixed in clays.

Consequently, clays containing pyrite and/or troilite impurities can be used as source of calcined clays, as soon as control measures are set up to ensure that

complete oxidation into stable iron oxide (hematite) took place during the calcination process.

**Acknowledgements** The authors would like to acknowledge financial support by the Swiss Agency of Development and Cooperation (SDC) Grant 81026665. The assistance of Dr. Diana Londono-Zuluaga on XRD analysis is acknowledged. The authors also acknowledge the motivation of the R.E.A.L. Project Team.

**Open Access** This article is licensed under a Creative Commons Attribution 4.0 International License, which permits use, sharing, adaptation, distribution and reproduction in any medium or format, as long as you give appropriate credit to the original author(s) and the source, provide a link to the Creative Commons licence, and indicate if changes were made. The images or other third party material in this article are included in the article's Creative Commons licence, unless indicated otherwise in a credit line to the material. If material is not included in the article's Creative Commons licence and your intended use is not permitted by statutory regulation or exceeds the permitted use, you will need to obtain permission directly from the copyright holder. To view a copy of this licence, visit <http://creativecommons.org/licenses/by/4.0/>.

## References

1. Scrivener KL, John V, Gartner EM (2016) Eco-efficient cements: potential, economically viable solutions for a low-CO<sub>2</sub>, cement-based materials industry. United Nations Environmental Programme (UNEP)
2. Zunino F, Martirena F, Scrivener K (2021) Limestone calcined clay cements (LC3). *ACI Mater J* 118:49–60. <https://doi.org/10.14359/51730422>
3. Antoni M, Rossen J, Martirena F, Scrivener K (2012) Cement substitution by a combination of metakaolin and limestone. *Cem Concr Res* 42:1579–1589. <https://doi.org/10.1016/j.cemconres.2012.09.006>
4. Bergaya F, Lagaly G (2013) Handbook of clay science, 2nd edn. Elsevier, Oxford
5. Fernandez R, Martirena F, Scrivener KL (2011) The origin of the pozzolanic activity of calcined clay minerals: a comparison between kaolinite, illite and montmorillonite. *Cem Concr Res* 41:113–122. <https://doi.org/10.1016/j.cemconres.2010.09.013>
6. Scrivener K, Martirena F, Bishnoi S, Maity S (2017) Calcined clay limestone cements (LC3). *Cem Concr Res*. <https://doi.org/10.1016/j.cemconres.2017.08.017>
7. Scrivener K, Avet F, Maraghechi H et al (2019) Impacting factors and properties of limestone calcined clay cements (LC<sup>3</sup>). *Green Mater* 7:3–14. <https://doi.org/10.1680/jgrma.18.00029>
8. Zunino F, Scrivener K (2020) Increasing the kaolinite content of raw clays using particle classification techniques for use as supplementary cementitious materials. *Constr Build Mater* 244:118335. <https://doi.org/10.1016/j.conbuildmat.2020.118335>
9. Martirena Hernández JF, Almenares-Reyes R, Zunino F et al (2020) Color control in industrial clay calcination. *RILEM Tech Lett* 5:1–7. <https://doi.org/10.21809/rilemtechlett.2020.107>
10. Zunino F, Boehm-Courjault E, Scrivener K (2020) The impact of calcite impurities in clays containing kaolinite on their reactivity in cement after calcination. *Mater Struct* 53:44. <https://doi.org/10.1617/s11527-020-01478-9>
11. Zunino F, Scrivener KL (2020) The effect of calcite and gibbsite impurities in calcined clay on its reactivity. In: Bishnoi S (ed) *Calcined clays for sustainable concrete*. Springer, Singapore, pp 357–362
12. Schmidt T, Leemann A, Gallucci E, Scrivener K (2011) Physical and microstructural aspects of iron sulfide degradation in concrete. *Cem Concr Res* 41:263–269. <https://doi.org/10.1016/j.cemconres.2010.11.011>
13. Paulik F, Paulik J, Arnold M (1982) Kinetics and mechanism of the decomposition of pyrite under conventional and quasi-isothermal—quasi-isobaric thermoanalytical conditions. *J Therm Anal* 25:313–325. <https://doi.org/10.1007/BF01912956>
14. Dunn JG, De GC, O'Connor BH (1989) The effect of experimental variables on the mechanism of the oxidation of pyrite. Part 1. Oxidation of particles less than 45 μm in size. *Thermochim Acta* 145:16
15. Dunn JG, De GC, O'Connor BH (1989) The effect of experimental variables on the mechanism of the oxidation of pyrite. Part 2. Oxidation of particles of size 90–125 μm. *Thermochim Acta* 155:15
16. Vázquez M, Moreno-Ventas I, Raposo I et al (2020) Kinetic evolution of chalcopyrite thermal degradation under oxidative environment. *Min Metall Explor* 37:923–932. <https://doi.org/10.1007/s42461-020-00204-x>
17. Scrivener K, Snellings R, Lothenbach B (2016) A practical guide to microstructural analysis of cementitious materials. CRC Press
18. ASTM C1897 (2020) Standard test methods for measuring the reactivity of supplementary cementitious materials by isothermal calorimetry and bound water measurements
19. Zhang Y, Li Q, Liu X et al (2019) A thermodynamic analysis on the roasting of pyrite. *Minerals* 9:220. <https://doi.org/10.3390/min9040220>
20. Tan Y, Wong K-W, Zhang Z, Ng KM (2017) In situ synthesis of iron sulfide embedded porous carbon hollow spheres for sodium ion batteries. *Nanoscale* 9:19408–19414. <https://doi.org/10.1039/C7NR06886G>
21. Schwertmann U (1991) Solubility and dissolution of iron oxides. *Plant Soil* 130:1–25

**Publisher's Note** Springer Nature remains neutral with regard to jurisdictional claims in published maps and institutional affiliations.

